Climate Dynamics (1993) 9:81–93

Climate Dynamics

Pinatubo eruption winter climate effects: model versus observations

H-F Graf[1], **I Kirchner**[1], **A Robock**[2], **I Schult**[1]

[1] Max-Planck-Institut für Meteorologie, Bundesstrasse 55, 20146 Hamburg, Germany
[2] Department of Meteorology, University of Maryland, College Park, MD 20742, USA

Received: 15 October 1992/Accepted: 22 February 1993

Abstract. Large volcanic eruptions, in addition to the well-known effect of producing global cooling for a year or two, have been observed to produce shorter-term responses in the climate system involving non-linear dynamical processes. In this study, we use the ECHAM2 general circulation model forced with stratospheric aerosols to test some of these ideas. Run in a perpetual-January mode, with tropical stratospheric heating from the volcanic aerosols typical of the 1982 El Chichón eruption or the 1991 Pinatubo eruption, we find a dynamical response with an increased polar night jet in the Northern Hemisphere (NH) and stronger zonal winds which extend down into the troposphere. The Azores High shifts northward with increased tropospheric westerlies at 60°N and increased easterlies at 30°N. Surface temperatures are higher both in northern Eurasia and North America, in agreement with observations for the NH winters of 1982–83 and 1991–92 as well as the winters following the other 10 largest volcanic eruptions since 1883.

Introduction

The eruption of Philippine volcano Mt. Pinatubo on June 15, 1991, was possibly the most sulfur-rich of this century, putting about 20 Mt of SO_2 into the stratosphere (Bluth et al. 1992), which converted to 40 to 50 Mt of sulfuric acid aerosols. Although conventional wisdom holds that volcanic aerosols produce cooling at the surface due to reduction of incoming solar radiation (and indeed that effect is to be expected on a two- to three-year timescale (Robock 1991)), the winter of 1991–92 (DJF) was warmer than average over North America and the Eurasian middle latitudes both in satellite derived temperatures of the lower half of the troposphere and in synoptic surface observations at the same time. Negative temperature anomalies were observed mainly over the eastern Mediterranean and over the northeastern part of North America, the Davis strait and Greenland. The question arises as to whether this anomaly pattern is produced by a deterministic process other than the reduction of shortwave radiation or is simply a manifestation of the internal climate variability. The possible effect of the coincidence of volcanic aerosol with an El Niño leading to the higher continental winter temperatures is discussed e.g., by Robock (1984) and Graf (1986). Experiments to study this effect in more detail are currently continuing and will be described in a forthcoming paper.

In the literature, some contradictive results have been published about the effect of volcanic aerosol on the climate of the cold season both from model studies and observations. Recent numerical volcano experiments with general circulation models (GCM) (Graf 1992; Hansen et al. 1992), in which the additional aerosol was introduced implicitly by reducing the solar radiation, shows the strongest climate signal during the warmer seasons. This is not surprising, since the simple linear reduction of incoming solar radiation as used in these studies has only a minor absolute effect in high latitudes during winter. Another experiment, mainly focused on the stratospheric processes (Rind et al. 1992) and including longwave and shortwave heating, found decreased tropospheric midlatitude westerlies. An energy-balance model (Robock 1984) and an annual cycle GCM calculation (Hansen et al. 1988, as analyzed by Robock and Liu in preparation) actually find enhanced cooling in the winter polar regions due to the sea ice/thermal inertia feedback. However there are observational studies that show winter warming after large eruptions over western North America (Lough and Fritts 1987) and northern Europe (Groismann 1985, 1992). A reanalysis of global temperature data (Robock and Mao 1992) reveals winter warming over large parts of Eurasia after all major volcanic

This paper was presented at the Second International Conference on Modelling of Global Climate Variability, held in Hamburg 7–11 September 1992 under the auspices of the Max Planck Institute for Meteorology. Guest Editor for these papers is L. Dümenil

Correspondence to: H-F Graf

eruptions of the last century since the eruption of Krakatau in 1883. The question thus arises, whether there are processes other than the direct effect of radiation which determine the climate response to volcanic aerosol during winter. One possibility is the dynamic coupling of stratosphere and troposphere, as has been shown with simple linear models (Geller and Alpert 1980; Schmitz and Grieger 1980). Numerical experiments (Boville 1986) showed, for instance, reduced meridional heat transport in the troposphere in the NCAR climate community model for conditions typical for stratospheric westerly circulation (cold polar and warm tropical stratosphere).

We therefore conducted a GCM experiment in which, in addition to the reduction of solar radiation at the top of the model atmosphere, heating rate anomalies were added in the stratosphere producing a generally realistic temperature anomaly field in the stratosphere. We want to study the atmospheric response to the volcanic disturbance keeping the ocean fixed. Therefore, any transitional effects from slowly varying parts of the climate system can be neglected. The atmospheric memory is, at best, two weeks. Since our main interest is in winter time conditions, the model was integrated in a "perpetual January"-experiment mode. Cumulative hydrological effects like the build-up of an enhanced snow cover and its effect on the Asian monsoon system are discussed in Graf (1992).

Experimental organisation

The stratospheric aerosol distribution observed in January 1983 in midlatitudes of the Northern Hemisphere, ten months after the eruption of El Chichón, is very similar to that seven months after Pinatubo in January 1992. The transmission of direct solar radiation for wavelengths of $\lambda = 0.3$ μm to 2.8 μm over Mauna Loa (see Climate Diagnostics Bulletin June 1992) is somewhat reduced in January 1992 ($q = 0.86$) compared with January 1983 ($q = 0.89$), and the column aerosol backscatter coefficient at ruby-wavelength ($\lambda = 0.69$ μm) at the same place is larger by a factor of two for January 1992. But, in middle latitudes of the Northern Hemisphere, lidar measurements of the aerosol column backscatter are comparable for both Januaries (Jäger personal communication see Fig. 1). Later in 1992 the Pinatubo aerosol became more effective in extinguishing solar radiation also in midlatitudes by a factor of 2 to 3 compared to the El Chichón aerosol. For our model simulation we used a prescribed aerosol distribution according to January 1992 observations, i.e., similar aerosol as in January 1983 for midlatitudes and more concentrated aerosol in low latitudes leading to a reduction in shortwave radiation as shown in Fig. 3 (dashed line). Lacis et al. (1992) found that the only important parameter for the net radiative forcing due to volcanic stratospheric aerosol is the optical depth. Therefore, lacking further detailed information about the optical properties of the January 1992 aerosol (e.g., effective radii of the particles), we used model calculations based on El Chichón to prescribe these.

The climate model used in our computations is the ECHAM2 GCM, used at the Max-Planck-Institut für Meteorologie for climate modelling research (Roeckner et al. 1992). We used the T21 version (horizontal resolution approximately 5.6°) with 19 vertical levels (top level at 10 hPa), the full diurnal cycle and standard physics, including cloud-radiation interactions. Sea surface temperature (SST) and sea ice extent are prescribed from climatology. An investigation of the relative effects of anomalous SST associated with the 1991–92 El Niño and the volcanic aerosol is in preparation.

Since the radiation scheme of the ECHAM2 climate model is unable to deal with variable aerosol concentrations, we decided to use the "anomaly forcing" technique which has previously been used to study the climate response to the smoke from the burning Kuwait oil wells (Bakan et al. 1991). This technique allows the inclusion of any radiational effects of trace gases or aerosols in the model by the use of an additional radiation model, which explicitly treats the species under investigation. In this case we used the δ-Eddington model, Bakan (1982), with the extensions for aerosol and ozone from Schult (1991). We ran this model parallel

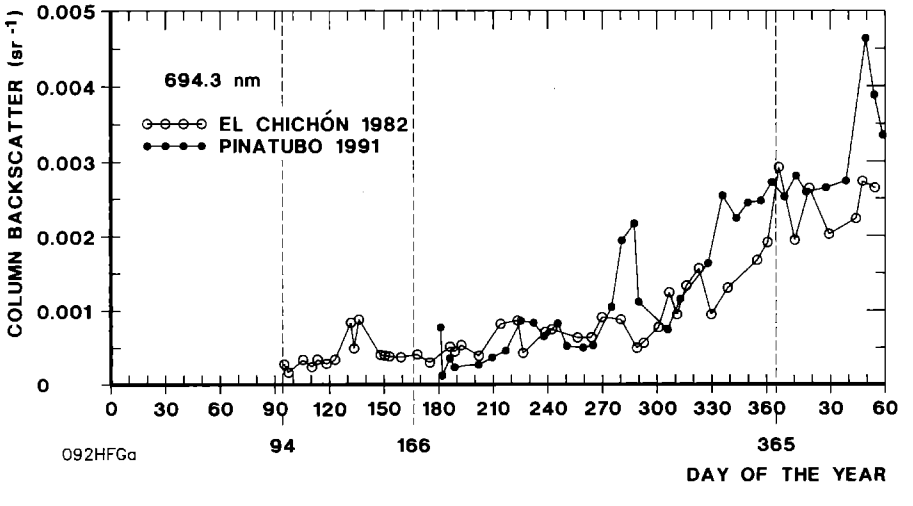

Fig. 1. Column backscatter for $\lambda = 694.3$ nm, Lidar observations over Garmisch-Partenkirchen (47.5°N, 11.0°E) after the eruption of El Chichón, April 4, 1982 (*open circles*) and Pinatubo, June 15, 1991 (*solid circles*) (from Jäger 1992, extended and redrawn). Day of Year 94 (166) is the day of the respective eruption

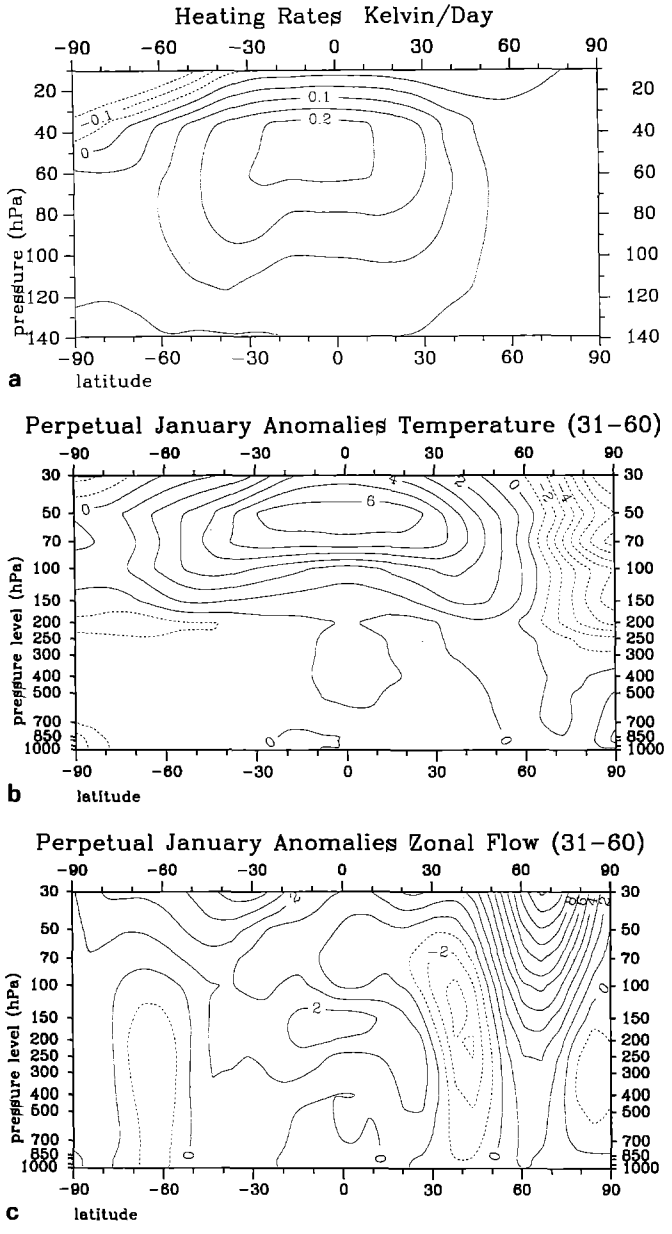

Fig. 2a–c. Cross sections of the zonal mean values of: **a** heating rate anomalies [K/d], as determined from the radiative transfer model for January 1983 or 1992; **b** temperature anomalies [K] for perpetual January experiment (month 31 to 60) minus control; **c** zonal wind anomalies [m/s] for perpetual January experiment minus control (month 31 to 60)

to the original ECHAM2 radiation code once with and once without the prescribed aerosol with the atmospheric conditions from the climate model. The flux differences of the two δ-Eddington computations are then added to the results of the original code. After six months of running this complete interactive radiation and circulation code we obtained mean monthly anomalies of the radiative fluxes and heating rates. The effect of the aerosol longwave radiation on the surface radiation balance was more than one order of magnitude less than the total effect. It will therefore (also in accordance with Lacis et al. 1992) be neglected in the computations described later.

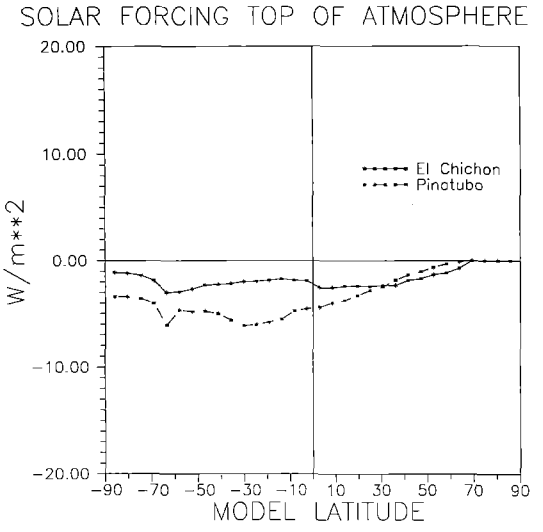

Fig. 3. Reduction of solar radiation [W/m^2] due to volcanic aerosol for January 1983 (*solid line*) and 1992 (*broken line*). The January 1992 values are used as solar forcing in the experiments

Since the fully interactive model increases the computation time for ECHAM2 by a factor of five, we avoided its explicit application in order to be able to run a series of experiments long enough for statistical investigations. Thus, we used the externally computed mean heating rate anomaly and the mean reduction of the shortwave radiation (Figs. 2a, 3) of the fully interactive model for a series of perpetual January simulations. The model was initiated using data from one arbitrarily chosen January 1 of the control experiment and integrated for 30 days. By doing this 60 times (each new 1st January being initialized with the fields of the 30th January of the former integration) we produced a series of 60 January simulations both for the disturbed (experiment) and the undisturbed (control) case.

To check the reliability of perpetual January simulations, we compared the mean model climate computed in the perpetual January mode with that of the 20 year transient (i.e., full annual cycle) control run. The basic features of the model climate of both Januaries are similar in midtropospheric circulation as well as in surface air temperature. Of course, there are some differences, but these are not statistically significant. It seems that the perpetual runs slightly favor the strong polar vortex mode. But, since in our study we only deal with anomalies, any systematic errors are filtered out.

Figure 4 gives an overview of the mean thermal and solar net radiation anomalies at the Earth's surface as the climate model produced for three different experiments for January conditions: Perm3 is our Pinatubo experiment, SST-2 is an El Niño experiment using the observed tropical (30°N to 30°S) sea surface temperature anomalies for January 1983, and Perm6 is the combined El Niño/Pinatubo experiment which will be discussed in a succeeding study. Anomalies of surface longwave as well as shortwave radiation are in the same order of magnitude for all experiments. In all cases there is net increase of longwave radiation in

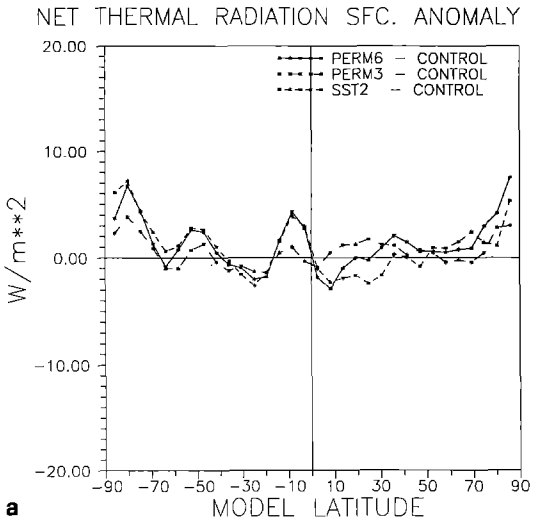

Fig. 4a,b. Net anomaly [W/m^2] at the surface for thermal **a** and solar **b** radiation for different permanent January experiments. *PERM3* is the actual volcano experiment, *SST2* is forced by tropical sea surface temperature anomalies as observed in January 1983, and *PERM6* is a combination of volcanic and SST forcings

middle and high latitudes. The pure El Niño experiment only leads to a meridional shift of cloud areas and therefore to a global mean zero effect of the shortwave anomaly, while the volcanic aerosol reduces solar radiation in the order of 5 to 7 W/m^2.

We inspected carefully the results for possible trends in the zonal mean of temperatures and geopotential and found that there were no strong trends detectable after few months. To check for the stability of any signal, we performed analyses with different subsets consisting of 30 Januaries each. We chose blocks of 30 succeeding Januaries and sets of randomly extracted Januaries, always excluding the first two months which show initial drift. All subsets gave the same principal patterns with only small variations in amplitudes and pattern. Here we will concentrate our discussion on the last half of the ensemble. The permanent January simulations are not independent of each other. This must be considered in the statistical tests by reducing the number of degrees of freedom. The effective number of degrees of freedom was computed for every gridpoint using the autocorrelation function. The resultant Bartels' number B (Bartels 1935) has a global mean value of B = 1.8 (B = 1.4) for the 2 m temperature (500 hPa height). This means that the effective degree of freedom is N_{eff} = N/B. This is consistent with the experience that the atmospheric memory is two weeks at the most. Trying to stay on the conservative side of estimates, we made the assumption that every second experiment January is independent. Consequently for a set of 30 Januaries we use an effective degree of freedom of 15. This leads to a slight underestimation of the significance of the anomaly amplitudes over most parts of the globe. Only over Antarctica is the Bartels' number larger, indicating some trend of the model results in this region.

Model results

Stratosphere

Although the model stratosphere has only a coarse resolution, the obtained results are comparable with observations and other model studies.

The zonal mean cross-section of the simulated temperature anomaly (Fig. 2b) is in good qualitative agreement with the corresponding observations from December 1991 (Fig. 5). Positive temperature anomalies are simulated and observed in low latitudes, and negative anomalies in the polar night region of the stratosphere. Although the heating rate anomaly is positive over the north pole (see Fig. 2a), the pole cools due to a dynamic effect; because of the intensified polar stratospheric vortex the meridional (poleward) heat transport decreases. The meridional temperature gradient

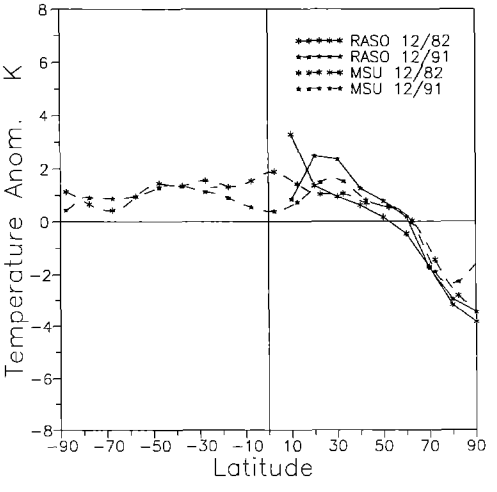

Fig. 5. Observed stratospheric December temperature anomaly from the 1982–91 mean after the eruptions of El Chichón (1982) and Pinatubo (1991), (*RASO,* radiosonde, 50 hPA, *solid lines*) (*MSU*, "lower stratosphere", *broken lines*)

between the tropics and the winter pole is strengthened in the lower stratosphere. In January 1992 a minor stratospheric warming occurred increasing the temperature in high northern latitudes by 5 to 6 K. Although stratospheric warmings in principle can be simulated by ECHAM2, it is not a predictable feature and is not reproduced by the model in this case.

Our results are also consistent with the study of Rind et al. (1992), who used the GISS model with an increased number of model layers (23 layers, top at 0.001 hPa). They investigated the effect of a homongenous aerosol layer of optical depth $\tau = 0.15$ on the zonal mean conditions in the middle atmosphere.

The dynamic effects in the stratosphere are primarily due to changes in the meridional temperature distribution. The mean zonal wind anomaly (Fig. 2c) shows an enhanced polar night jet in the stratosphere with anomalies up to 10 m/s. These westerly anomalies also penetrate downward into the troposphere resulting in a poleward shift of the upper tropospheric westerly jet in the Northern Hemisphere.

Troposphere

The model simulates a significant reduction of the variance of the geopotential height of the 200, 500 and 850 hPa levels over the whole North Atlantic region. This holds also for the variances of the zonal wind field and temperature (the latter mainly in the lower troposphere) for the complete set of the experiment (Fig. 6) as well as for subsets. This is especially clear for the geopotential over the Azores high, over Labrador and southern Greenland. No significant signal is detectable elsewhere applying the F-test, or the variance is increased in the experiment (Fig. 6).

A local *t*-test was used to test for the significance of the amplitudes of the zonal wind, geopotential height and 2 m-temperature anomalies in different sets of 30 experiment months. Here we will focus on the results for the Januaries 31 to 60, i.e., on the second half of the experiment. Principially, the anomaly patterns were similar in the other sets of each 30 Januaries.

In addition to the *t*-test, and in order to test for the difference of the distribution functions of the control and the experiment, a recurrency analysis (von Storch and Zwiers 1988) was also applied to several sets of Januaries. The *t*-test and recurrency test give comparable results, especially concerning the areas of statistically significant signals. In each set the pattern of anomalies of the geopotential heights is similar throughout the troposphere.

The largest amplitudes of the geopotential heights in all tropospheric levels occur over the North Atlantic, where the pattern indicates a northward shift of the tropospheric circulation (Fig. 7). The Azores high is displaced northward by about 15° and the Icelandic low shifted towards Greenland. This pattern is significant ($\beta = 0.05$) following the *t*-test and recurrent in all sets as are the negative tropical geopotential anomalies, mainly in the middle troposphere. The most prominent signal is the anticyclonic anomaly in the area of the northward shifted Azores high. Thus, the area of strongest and recurrent circulation anomalies is the North Atlantic. This holds for the whole troposphere. The structure of the anomaly patterns throughout the troposphere suggests a barotropic response. It is suggested that the interaction between the strengthened stratospheric polar night jet with tropospheric lee effects of the Rocky Mountains is responsible for the strongest response of the circulation to the aerosol forcing over the North Atlantic. The primary effect may be a change in the stationary planetary wave pattern.

The westerlies over the North Atlantic are shifted northwards resulting in westerly wind anomalies around 60°N and easterly anomalies at 30°N (Fig. 8). This pattern again is stable throughout the whole troposphere. It is also combined with a significant reduction of the variance of the zonal wind component as is obvious from the F-test. Accordingly the North Atlantic centers of action shift northward.

In the tropics, the anomalies of the zonal wind component change sign from the lower to the upper troposphere. In both sets, over the eastern equatorial Pacific in the lower (upper) troposphere easterly (westerly) wind anomalies are found. This indicates a slightly strengthened Walker circulation over the eastern equatorial Pacific during winter.

The meteorological parameter which normally is of interest in connection with violent volcanic eruptions is the surface air temperature. Figure 9 (lower panel) shows the mean anomaly of this parameter, again for the last 30 Januaries of our experiment. The main features, however, are similar also for other subsets of the 60 January integration after a few months of initial drift. The *t*-test shows a major significant area of cooling over North Africa and the Middle East, strong cooling over Greenland and parts of China. In the Southern Hemisphere the only significant signals are the cold southern tip of South America and Antarctic cooling. Significant warming only occurs in the Barents Sea. Here one of the model's restrictions is apparent, i.e., the fixed sea ice coverage and temperature. This, in part, prevents the development of positive anomalies of the 2 m temperature. In the free troposphere (e.g., in 850 hPa, Fig. 9, middle panel), where the surface conditions are less important and the transport processes become dominant, the warming is significant over large parts of the Arctic ocean north of Siberia and the warm anomaly reaches further south over Asia.

Tropospheric observations

In order to compare our simulation of the impact of the Pinatubo (or another similar volcanic eruption) stratospheric aerosol on climate with global observations data, we used the 500 hPa geopotential height anomalies as analyzed by the US National Weather Service, the satellite observed lower tropospheric tem-

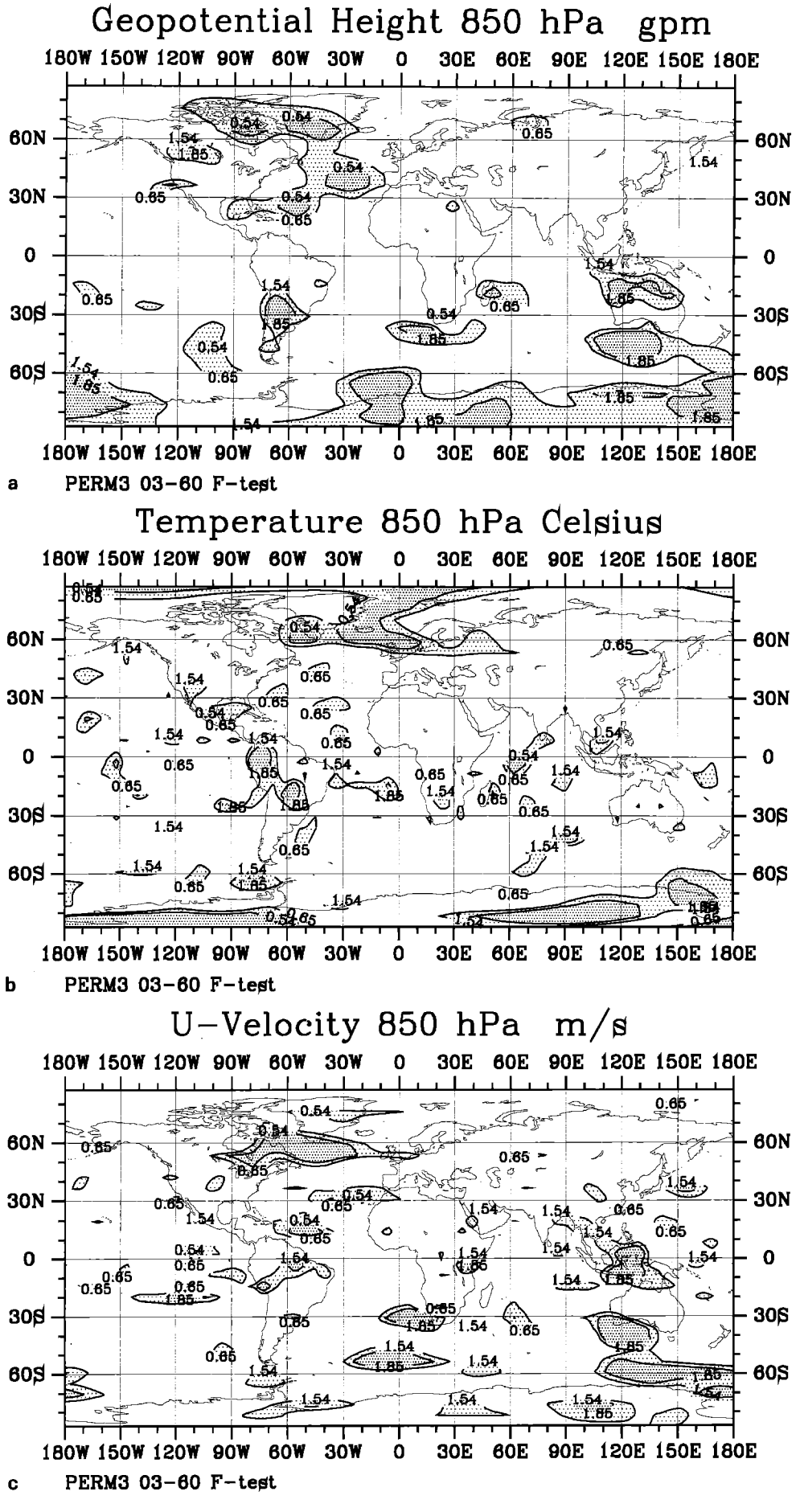

Fig. 6. Changes in local variance (F-test) at the 850 hPa level for: Geopotential height (*top*), zonal velocity (*middle*), and temperature (*bottom*) for the permanent January experiment. *Shading* indicates significant differences between experiment and control. Values larger (smaller) than 1 means that the variance in the experiment is larger (smaller) than in the control

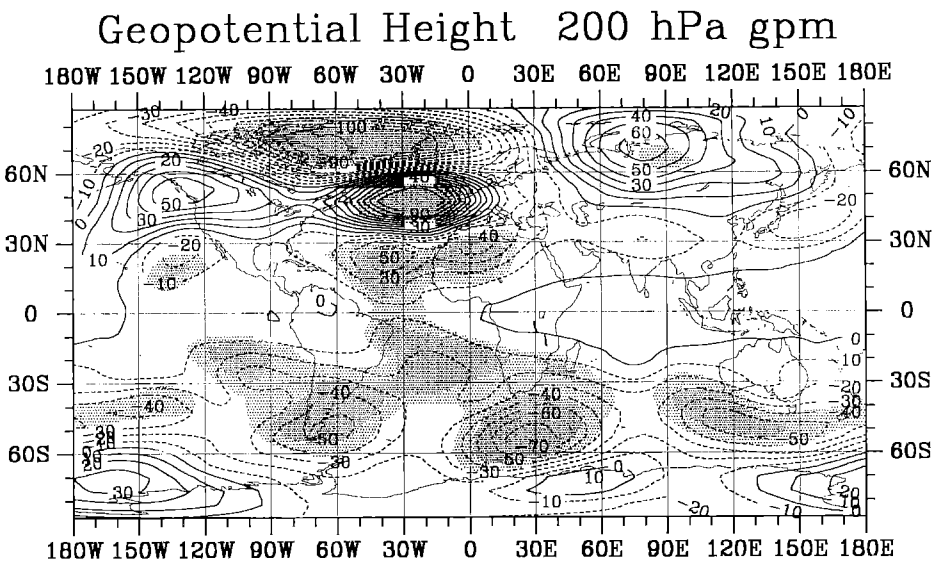

a Perm3–Control (31–60) 5% and 1% significance

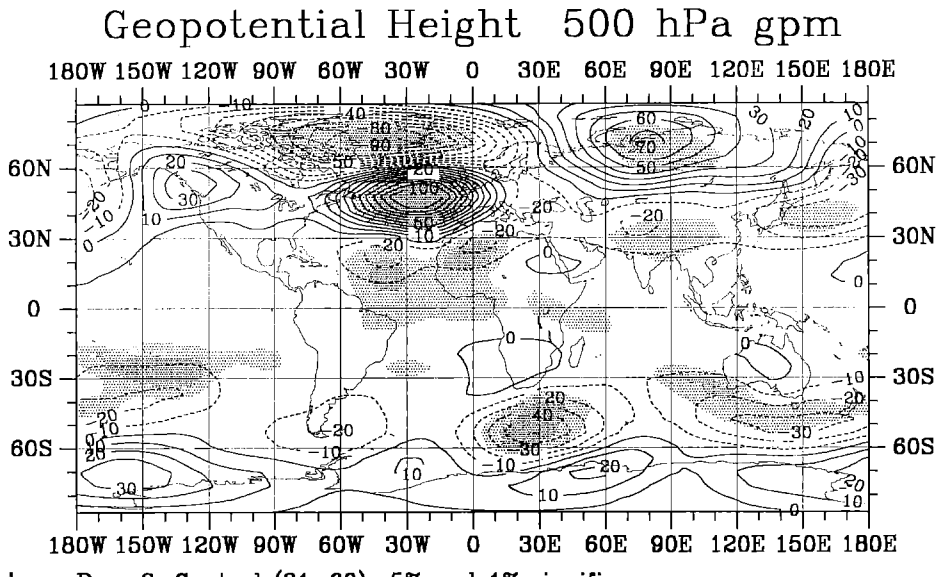

b Perm3–Control (31–60) 5% and 1% significance

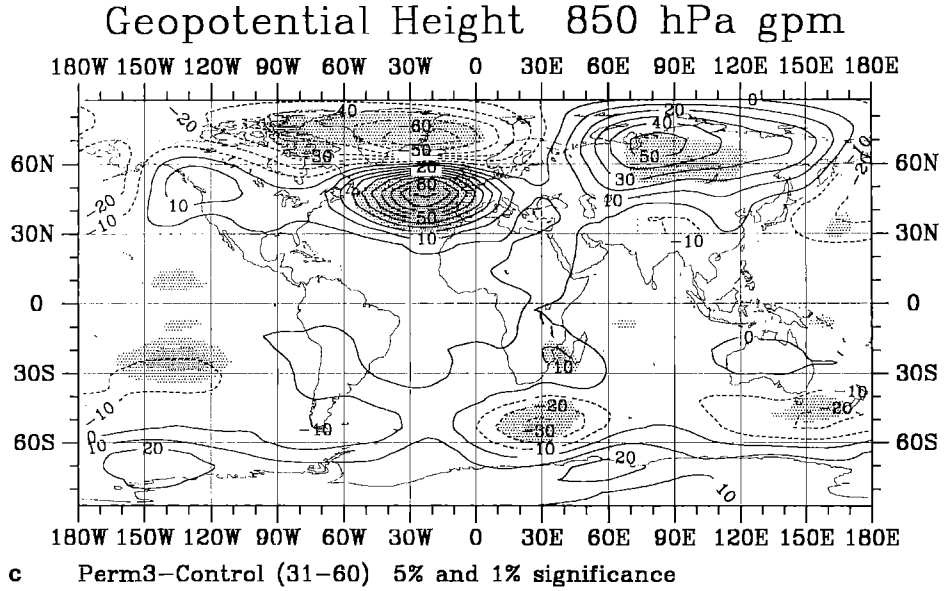

c Perm3–Control (31–60) 5% and 1% significance

Fig. 7. Anomalies of the geopotential height at different tropospheric levels. *Shading* indicates statistically significant (error chance 5%) differences between experiment and control for months 31 to 60 on the basis of a local *t*-test, degrees of freedom reduced to 15

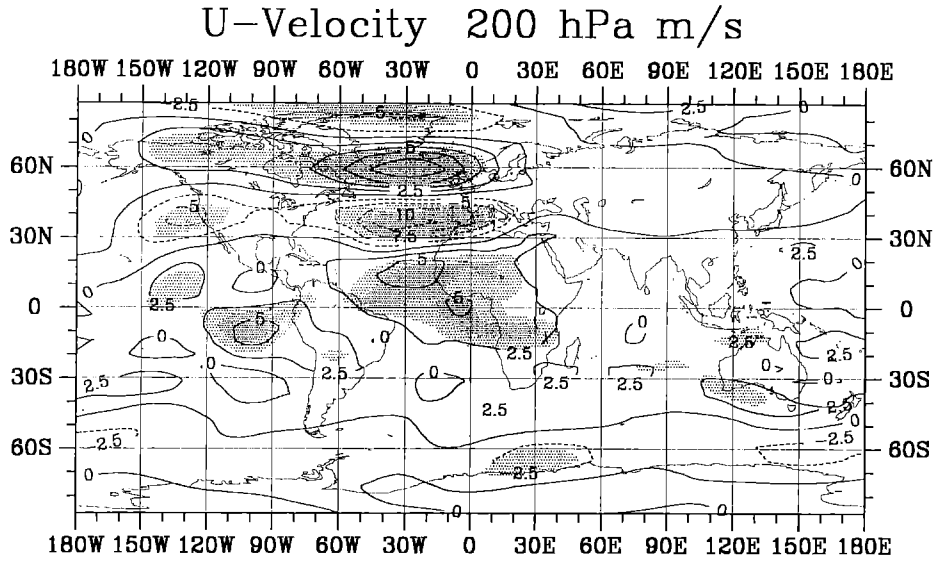

a Perm3–Control (31–60) 5% and 1% significance

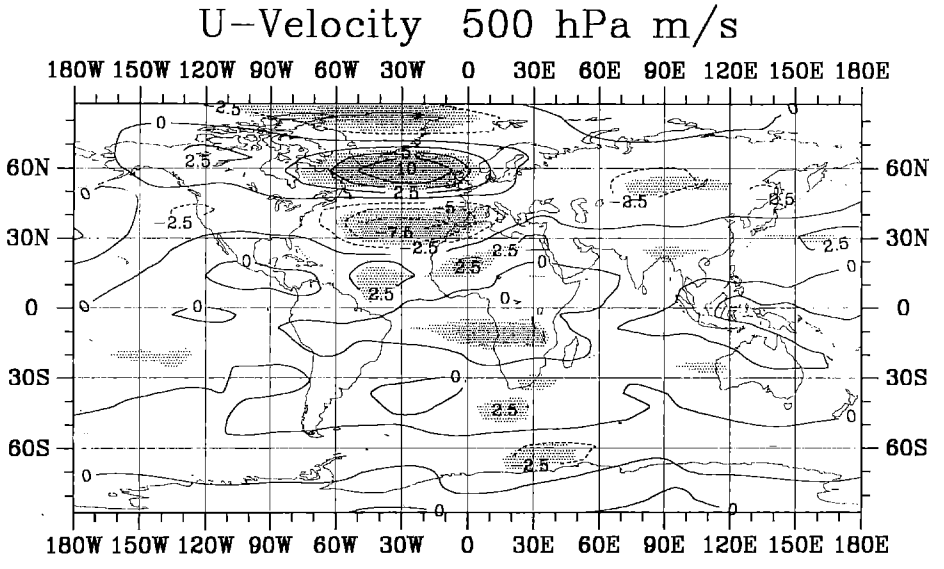

b Perm3–Control (31–60) 5% and 1% significance

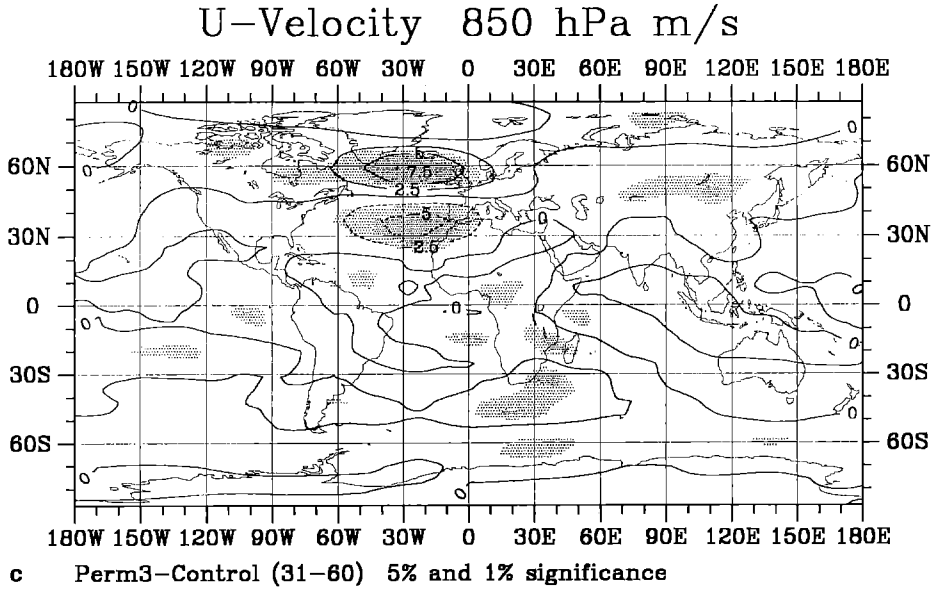

c Perm3–Control (31–60) 5% and 1% significance

Fig. 8. Anomalies of the zonal wind component at different tropospheric levels. *Shading* indicates statistically significant (error chance 5%) differences between experiment and control for months 31 to 60 on the basis of a local *t*-test, degrees of freedom reduced to 15

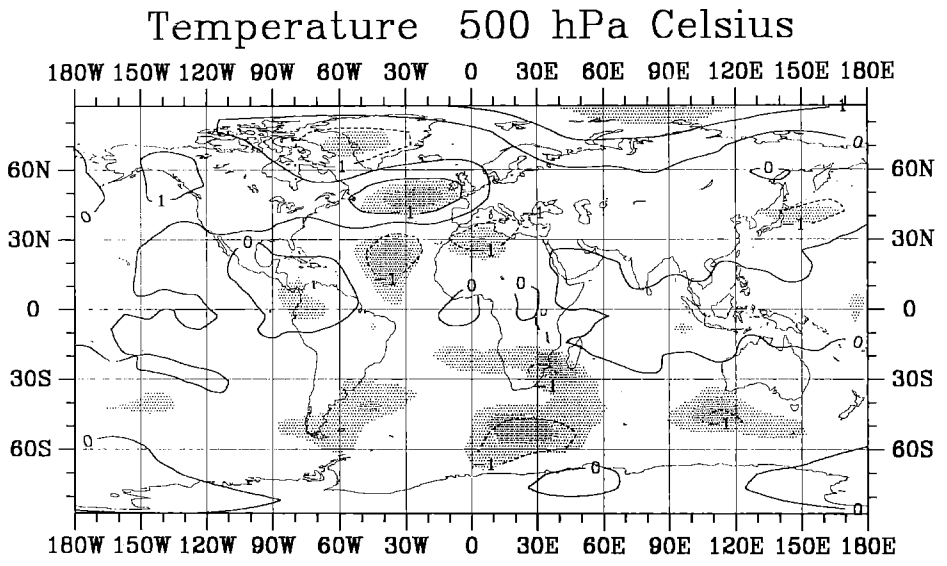

a Perm3–Control (31–60) 5% and 1% significance

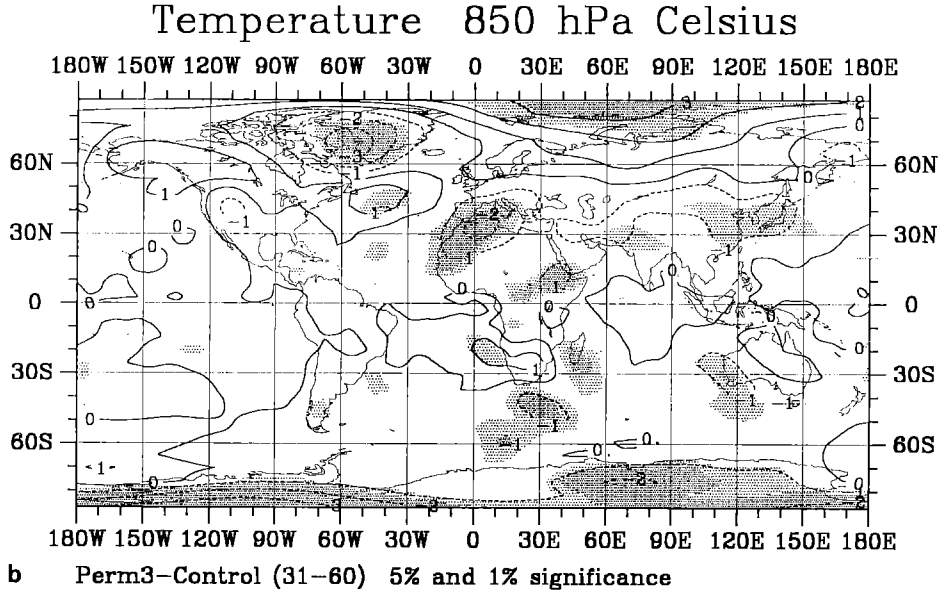

b Perm3–Control (31–60) 5% and 1% significance

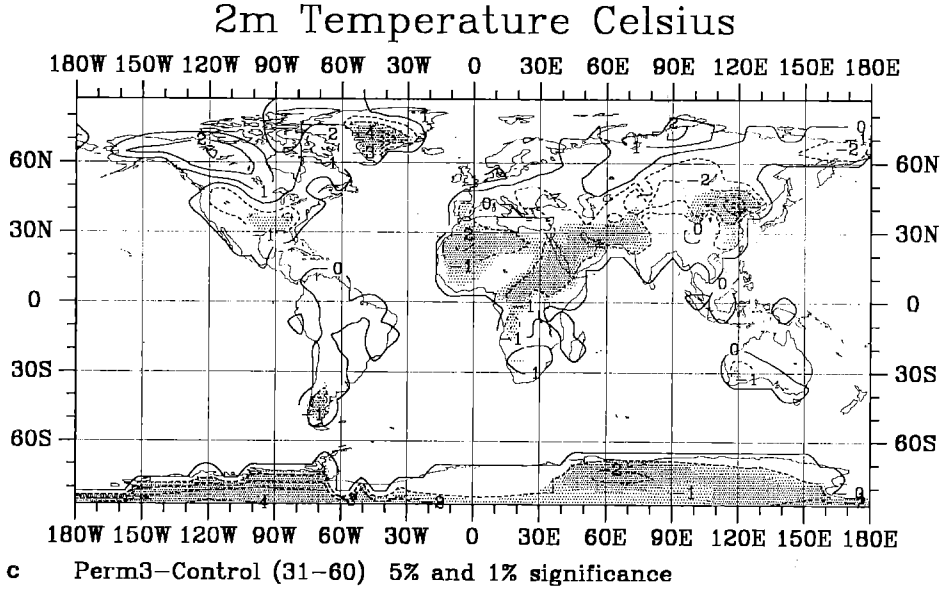

c Perm3–Control (31–60) 5% and 1% significance

Fig. 9. Anomalies of the air temperature in the lower troposphere. *Shading* indicates statistically significant (error chance 5%) differences between experiment and control for months 31 to 60 on the basis of a local *t*-test, degrees of freedom reduced to 15

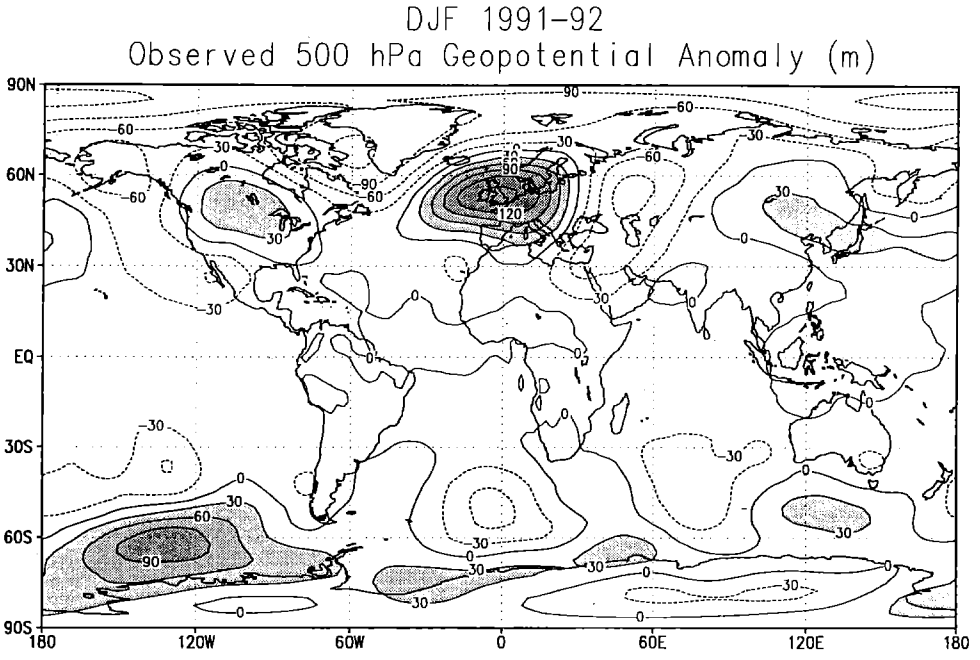

Fig. 10. Anomaly of the 500 hPa geopotential height as analyzed by the US NWS, mean of December 1991 through February 1992. Anomalies calculated from mean 1982–1990

Table 1. Pattern correlation coefficients (area weighted, multiplied by 100) between observed and simulated meteorological fields

Parameter	Global	N Hemisphere	90°W–90°E	0°–180°E	0°–180°W
MSU-temperature					
1:1	18	57	39	54	60
Optimal	29	57	62	56	63
500 hPa					
1:1	35	39	1	—29	68
Optimal	37	40	41	—46	70

A 1:1 correlation means that no spatial shift is allowed, "optimal" correlation allows for 2 gridpoints shift in all directions to get a best fit. All fields were interpolated to the T21 grid before being analyzed. Mean of the experiments 03–60 used

perature from the Microsounding Unit (MSU) (Spencer and Christy personal communication), and (to a certain degree) synoptic observations collected by the Seewetteramt of the Deutscher Wetterdienst. The last data set is based on a non-uniform distribution of stations with large gaps over the oceans. This produces serious problems when the data are interpolated to a coarse map such as the T21 grid. Thus, these data are used only for qualitative comparisons.

The MSU temperature data use the temperature dependence of the microwave emission of oxygen molecules. For the tropospheric signal, calibrated MSU channel 2 (53.74 GHz) brightness temperatures are combined with a weighting function describing the vertical sensitivity to thermal emission by molecular oxygen in the atmosphere. The main part of the signal we used is from the layer between the Earth's surface and 400 hPa (with a peak at 700 hPa), i.e., from the lower part of the troposphere rather than from the Earth's surface. The spatial resolution of these observations is in the order of 10°, even though the data are published on a 2.5° grid (Spencer et al. 1990).

In order to compare with previous violent volcanic eruptions, the surface temperature data set from Jones et al. (1988) was also used (see Robock and Mao 1992).

An inspection of the mean December 1991 through February 1992 500 hPa height anomaly (Fig. 10) shows some similarity between our simulation and observed anomalies (see also Graf et al. 1993): The strongest anomalies occur in the Atlantic region. The simulated anomalies are generally weaker than the observed ones and a tendency to a westward displacement is characteristic. Such zonal (westward) displacements (compared with observations) of the mean circulation features are common in low resolution GCMs, resulting mainly from the smooth orographic representation (Sausen 1992, personal communication). The negative anomaly over Greenland exists in both fields (for the simulated anomaly see Fig. 6), while the observed center of the positive geopotential anomaly is shifted eastwards to England. Both in the observations and in the simulation a trough develops over Eastern Europe/Western Asia, which also has a more westerly position than in the observations. The pattern anomaly correlation (Table 1) is between 0.37 for the globe and 0.40 for the Northern Hemisphere if we use the mean pattern of the experiments 03-60. As stated, subsets have

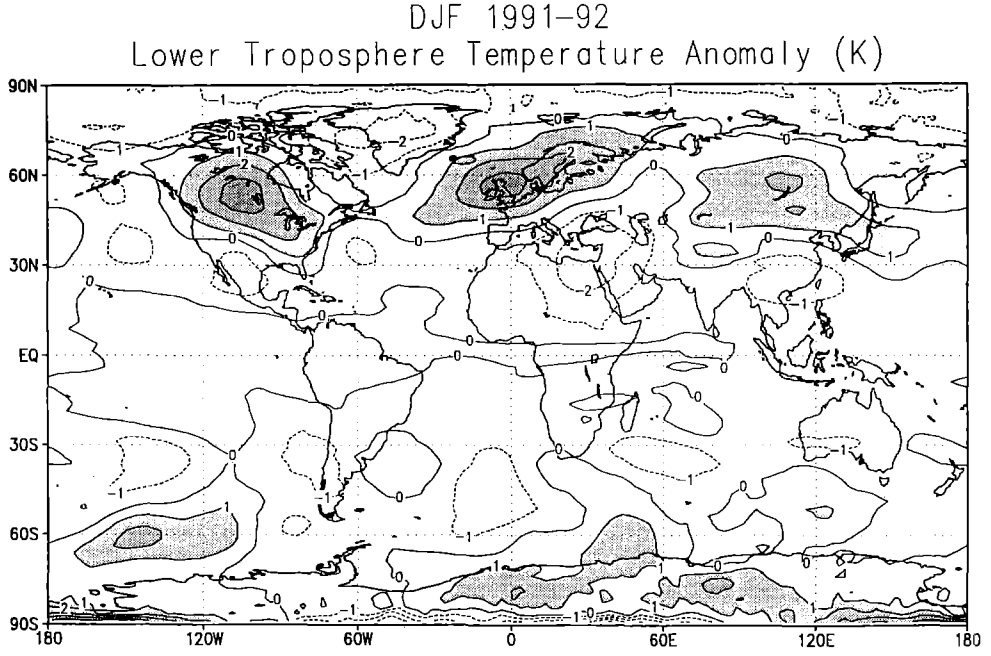

Fig. 11. Anomaly of the air temperature near surface [K] as observed December 1991 through February 1992 from MSU satellite data. Anomalies calculated from mean for 1982–1990

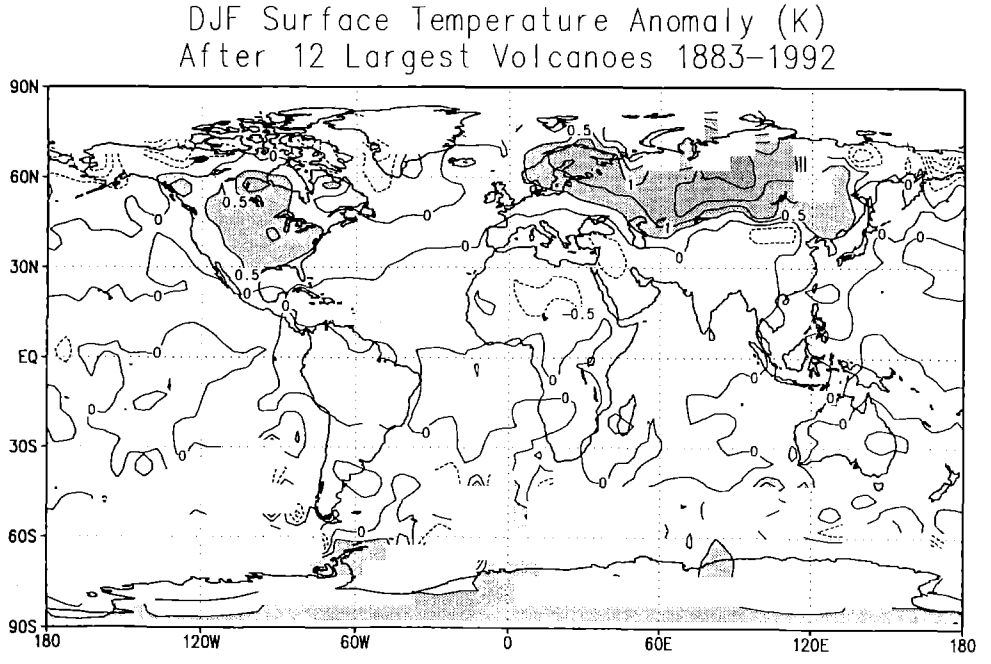

Fig. 12. Observed December through February mean temperature anomaly after the twelve largest volcanic eruptions of the last century (Data from Jones 1988, updated, Jones, personal communication)

shown the same patterns. This means that only about 15% of the total North Hemispheric observed spatial variance of the 500 hPa field of the middle troposphere in winter 1991–92 can be explained by the volcanic impact alone. We get much better results for the Western Hemisphere (180°W to 0°) where this value can be improved to 49% ($r=0.70$). Over Siberia the patterns of 500 hPa geopotential height anomalies do not agree well because of a simulated high over North Siberia which is not observed in winter 1991/92.

For the lower tropospheric temperature (Fig. 11), reasonable agreement between simulations and observations in winter 1991–92 is found for the Northern Hemisphere again. The "optimal" pattern correlations are between $r=0.56$ and $r=0.63$ for different subareas of the Northern Hemisphere (Table 1), resulting in $r=0.57$ for the whole Northern Hemisphere. This means that about 35 to 40% of the total spatial variance of the observed 2 m temperature can be explained by the volcanic forcing alone. The model reproduced especially well the cooling over Greenland and North Africa. Some of the warming of the middle and high latitudes of the northern continents, which is seen in both patterns, is also modelled in the right place, although not significant with respect to the amplitude because of the high variability of the temperature in these latitudes in the control run.

The good agreement between the model simulation and the observations in winter 1991/92 still could be coincidental. This might be excluded if similar anomaly

patterns evolved after other volcanic eruptions as well.

An examination of the near surface temperature data set from Jones et al. (1988 updated, Jones personal communication) after the twelve most violent volcanic eruptions of the last century (Fig. 12) also shows good agreement with our simulations. For the six tropical volcanoes (Krakatau, Sta. Maria, Agung, Fuego, El Chichón and Pinatubo) the anomalies are for the following boreal winter, for the six high latitude volcanoes (Novarupta, Tarawera, Bandai, Ksudach, Cerro Azul and Bezymianny) anomalies are for the second winter after the eruption to allow time for the aerosols to reach the tropical stratosphere. The anomalies are calculated from the 1951 to 1980 means as differences from low pass (cut-off 10 years) filtered data. The pattern after every volcano is virtually the same as the mean effect shown in Fig. 12, apart from some differences over North America for winters with and without El Niños. The best pattern correlation between the composite signal of post eruption winter temperatures and our simulation is found for the sector between 90°W and 90°E on the Northern Hemisphere ($r=0.35$). There is a zero pattern correlation for the western half of the North Hemisphere and only $r=0.21$ for the eastern half.

Conclusions

The perpetual January GCM simulation has shown that the stratospheric aerosol produced by a violent and sulfur-rich volcanic eruption can alter the stratospheric and tropospheric climate conditions significantly. Using the "anomaly forcing" technique the stratospheric forcing due to the aerosol (which is not included in the original GCM) can be simulated in accordance with other model simulations and observations. The stratospheric winter signal can be described as a significant warming of the aerosol containing layers in the tropics and midlatitudes due to absorption of radiative energy. This warming increases the poleward meridional temperature gradient, leads to an increased polar night jet, reduced meridional heat transport and therefore a cooling tendency in the stratosphere over the winter pole.

In this study the tropospheric signal was found to be zonally non-uniform. It is strongest over the North Atlantic and consists of enhanced west winds over high latitudes (around 60°N), strengthened zonal heat and moisture transport in higher latitudes and a northward shift of the Azores high. The areas of strongest anomalies also show significantly reduced variance of the parameters.

A temperature anomaly field was found in the lower troposphere, which (in its main features) is very similar to observations during the winter 1991–92. Similar anomalies were observed also during other post volcano winters. There is a significant cooling over Greenland and North Africa/Middle East. In agreement with observations some warming tendency with a maximum amplitude of about 2K is seen in the mean results over North America and northern Eurasia. This positive temperature anomaly cannot be proved to be statistically significant because of the large natural variability of surface temperature in these latitudes. This warm anomaly is supported by observations following historic eruptions (Robock and Mao 1992) and it determines the high pattern correlation found between simulation and observations.

The simulated and observed temperature anomalies following a violent volcanic eruption partly contradict the findings based on linear multiple regression analysis (Cress and Schönwiese 1991) and energy balance models (Robock 1984). The results underline the importance of nonlinear and dynamic responses of the atmosphere to external forcing.

Acknowledgements. We thank John Christy, Phil Jones and Karin Labitzke for providing the temperature data. We are grateful to M. Grunert for preparing Fig. 1, to Jiaoping Mao for producing the analyses in Fig. 12 and to Brian Doty for the GrADS software for Fig. 10 to 12. We thank Huug van den Dool and John Janowiak for the 500 hPa data. Data are from the Climate Analysis Center of the National Meteorological Center of NOAA. Comments of Lennart Bengtsson and Mojib Latif on a first version of the manuscript helped clarify the presentation. This work was partially supported by the Bundesministerium für Forschung und Technologie (No. 07-KFT-86/2), NSF grant ATM-8920590 and NASA grant NAG 5-1835.

References

Bakan S, Chlond A, Cubasch U, Feichter J, Graf H, Grassl H, Hasselmann K, Kirchner I, Latif M, Roeckner E, Sausen R, Schlese U, Schriever D, Schult I, Schumann U, Sielmann F, Welke W (1991) Climate response to smoke from the burning oil wells in Kuwait. Nature 351:367–371

Bakan S (1982) Strahlungsgetriebene Zellularkonvektion in Schichtwolken. Dissertation, University of Hamburg, Germany

Bartels J (1935) Random fluctuations, persistence, and quasipersistence in geophysical and cosmical periodicities. Terr Magn Atmos Electron 40:1–60

Boville BA (1986) The influence of the polar night jet on the tropospheric circulation in a GCM. J Atmos Sci 41:1132–1142

Bluth GJS, Doiron SD, Krueger AJ, Walter LS, Schnetzler CC (1992) Global tracking of the SO_2 clouds from the June, 1991 Mount Pinatubo eruptions. Geophys Res Lett 19:151–154

Cress A, Schönwiese C-D (1990) Vulkanische Einflüsse auf die bodennahe und stratosphärische Lufttemperatur der Erde. Ber Inst f Meteorol Geophysik Univ Frankfurt/Main 82, 148 pp

Geller MA, Alpert JC (1980) Planetary wave coupling between the troposphere and the middle atmosphere as a possible sun-weather mechanism. J Atmos Sci 37:1197–1215

Graf HF (1986) On El Niño/Southern Oscillation and Northern Hemispheric temperature. Gerlands Beitr Geophys 95:63–75

Graf HF (1992) Arctic radiation deficit and climate variability. Clim Dyn 7:19–28

Graf HF, Perlwitz J, Kirchner I (1993) Northern Hemisphere tropospheric mid-latitude circulation after violent volcanic eruptions. Geophys Res Lett (in press)

Groismann PY (1985) Regional climatic consequences of volcanic eruptions. Meteorol Hydrol 4:39–45 (in Russian)

Groisman PY (1992) Possible regional consequences of the Pinatubo eruption: an empirical approach. Geophys Res Lett 19:1603–1606

Hansen J, Lacis A, Ruedy R, Sato M (1992) Potential climate impact of Mount Pinatubo eruption. Geophys Res Lett 19:215–218

Jäger H (1992) The Pinatubo cloud observed by Lidar over Garmisch-Partenkirchen. Geophys Res Lett 19:191–194

Jones PD (1988) Hemispheric surface air temperature variations: recent trends and an update to 1987. J Clim 1:654–660

Jones PD, Wigley TML, Folland CK, Parker DE, Angel JK, Lebedeff S, Hansen JE (1988) Evidence for global warming in the past decade. Nature 332:790

Lacis A, Hansen J, Sato M (1992) Climate forcing by stratospheric aerosols. Geophys Res Lett 19:1607–1610

Lough JM, Fritts HC (1987) An assessment of the possible effects of volcanic eruptions on North American climate using treering data, 1602–1900 A.D., Clim Change 10:219–239

Rind D, Balachandran NK, Suozzo R (1992) Climate change and the middle atmosphere. Part II: the impact of volcanic aerosols. J Clim 5:189–208

Robock AD (1984) Climate model simulations of the El Chichón eruption. Geofis Int 23:403–414

Robock AD (1991) The volcanic contribution to climate change of the past 100 years. In: Schlesinger ME (ed) Greenhouse-gas-induced climate change: a critical appraisal of simulations and observations. Elsevier, Amsterdam, pp 429–444

Robock A, Mao J (1992) Winter warming from large volcanic eruptions. Geophys Res Lett 12:2405–2408

Roeckner E, Arpe K, Bengtsson L, Brinkop S, Dümenil L, Esch M, Kirk E, Lunkeit F, Ponater M, Rockel B, Sausen R, Schlese U, Schubert S, Windelband M (1992) Simulation of the present-day climate with the ECHAM model: impact of model physics and resolution. MPI Report No 95

Schmitz G, Grieger N (1980) Model calculations of the structure of planetary waves in the upper troposphere and lower stratosphere as a function of the wind field in the upper stratosphere. Tellus 32:207–214

Schult I (1991) Bildung und Transport von Aerosolteilchen in der Stratosphäre und ihre Bedeutung für den Strahlungshaushalt. Examensarbeit No 11, Max-Planck-Institut für Meteorologie, Hamburg

Spencer RW, Christy JR, Grody NC (1990) Global atmospheric temperature monitoring with satellite microwave measurements: method and results 1979–84, J Clim 3:1111–1128

Storch H von, Zwiers FW (1988) Recurrence analysis of climate sensitivity experiments. J Clim 1:157–171